Desalination and Water Treatment
www.deswater.com

doi: 10.5004/dwt.2022.28271

253 (2022) 270–284
March

Supporting performance of magnetic-liquid double suspension bearing under wear of magnetic poles

Jianhua Zhao[a,b], Weidong Yan[a], Fang Han[a], Xuchao Ma[a], Lanchun Xing[a], Guojun Du[b,*]

[a]*Fluid Power Transmission and Control Laboratory, Yanshan University, Qinhuangdao 066004, China, emails: zhaojianhua@ysu.edu.cn (J. Zhao), yanweidongysu@163.com (W. Yan), hanfang7291@foxmail.com (F. Han), mxc18630334372@163.com (X. Ma), xinglanchun@foxmail.com (L. Xing)*
[b]*College of Civil Engineering and Mechanics, Yanshan University, Qinhuangdao 066004, China, email: gaodr@ysu.edu.cn/dugj2002@ysu.edu.cn (G. Du)*

Received 14 June 2021; Accepted 30 January 2022

ABSTRACT

As a new type of suspension bearing, magnetic-liquid double suspension bearing (MLDSB) is mainly supported by electromagnetic suspension and supplemented by hydrostatic supporting. Its supporting capacity and stiffness can be greatly improved, and then it is suitable for the occasions of medium speed, heavy load. Due to the small liquid film thickness (It is smaller nearly 10 times than air-gap), the eccentricity, crack, bending of the rotor, the assembly error, it is easy to cause clearance-rubbing fault between the rotor and stator. The coating can be worn and peeled, the operating stability can be reduced, and then it is one of the key problems of restricting the development and application of MLDSB. Therefore, a new method for soft measurement of wear of magnetic pole is presented, and the expressions of bearing stiffness and damping in the magnetic pole coating-wear mode and the dynamic equation of two DOF rubbing system are established. The influence of wear amount on the supporting performance and dynamic behavior under different wear conditions is simulated numerically, and the supporting performance is restored by adjusting the electromagnetic control parameters. The study shows that supporting performance and operation stability of bearing system are reduced due to wear of the magnetic poles, and wear of *y*-direction is the most serious, bifurcation and chaos occur in the system, and secondary wear occurs between the magnetic pole and flux sleeve. By measuring the pressure and flow rate of the static pressure system in real time, the wear amount of each magnetic pole coating can be predicted effectively, which provides a theoretical basis for the safe and stable operation of MLDSB. According to the wear value of each magnetic pole coating, the control parameters of the electromagnetic system are adjusted to make the supporting performance of the MLDSB return to the initial theoretical state to prevent secondary wear. The research can provide a theoretical basis for the safe and stable operation of MLDSB.

Keywords: Magnetic-liquid double suspension bearing; Wear of magnetic pole; 2-DOF rubbing system; Supporting performance; Bifurcation and chaos

1. Introduction

The high-pressure desalination pump is the core power equipment that provides reverse osmosis pressure and flow in the reverse osmosis desalination process. It is the "heart" of the reverse osmosis desalination project and directly affects the energy consumption and operational reliability of the reverse osmosis desalination process. And the reverse osmosis desalination process is shown in Fig. 1.

* Corresponding author.

With the rapid development of the social economy and the continuous increase of population, the lack of fresh water resources has become more and more serious, forcing seawater desalination projects to gradually develop in the direction of high power and large-scale [1].

The bearing system is a key core component to ensure the supporting performance and operational stability of seawater desalination high-pressure pump, which directly affects the operation status, maintenance period and service life [2]. At present, the high-pressure pumps of medium and large seawater desalination projects are all multi-stage centrifugal pumps, which are supported by sliding bearings that use seawater as the lubricating medium. However, due to the low viscosity and special physical and chemical properties of seawater, it is difficult to form the lubricating film of seawater-lubricated friction bearings, and the supporting capacity and stiffness of liquid film are poor, which has become one of the consensus problems in this field [3].

To sum up, the research group made efforts to innovate on the basis of previous research results and experience, and for the first time introduced electromagnetic levitation theory into seawater lubricated bearings to form magnetic-liquid double suspension bearing (MLDSB), which is suitable for seawater desalination high-pressure pump system.

MLDSB is composed of bracket, motor, coupling, multi-diameter shaft, journal bearing unit, axial bearing unit, journal loading motor, axial loading motor and so on as Fig. 2 [4].

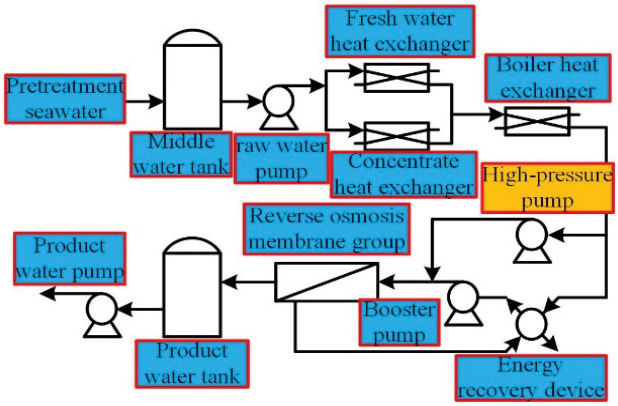

Fig. 1. Process flow of reverse osmosis seawater desalination.

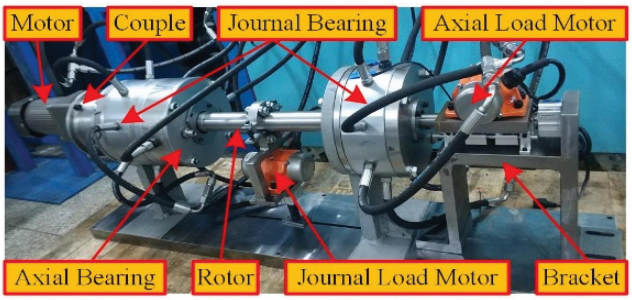

Fig. 2. Experimental table of MLDSB.

The radial element of MLDSB is composed of step shaft, magnetic sleeve, supporting chamber, magnetic pole, inlet pipe, shell, coil, outlet, and so on as shown in Figs. 3 and 4 [4]. The material of magnetic pole and magnetic sleeve are cold-rolled non-oriented silicon-steel, and chromium layer is coated in order to solve the problem of matrix corrosion in the lubricants for a long time [5].

The control principle of MLDSB is shown in Fig. 5 [4]. Constant-pressure supply model is adopted in the hydrostatic supporting system, and throttle valves connecting the upper and lower supporting cavities are connected by differential module. PD control is adopted in electromagnetic supporting system, and upper and lower coils are connected through differential connection module [6]. When the rotor is radial offset by external interference, its displacement is

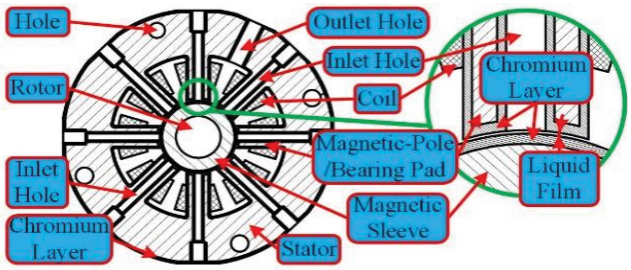

Fig. 3. Radial unit of MLDSB.

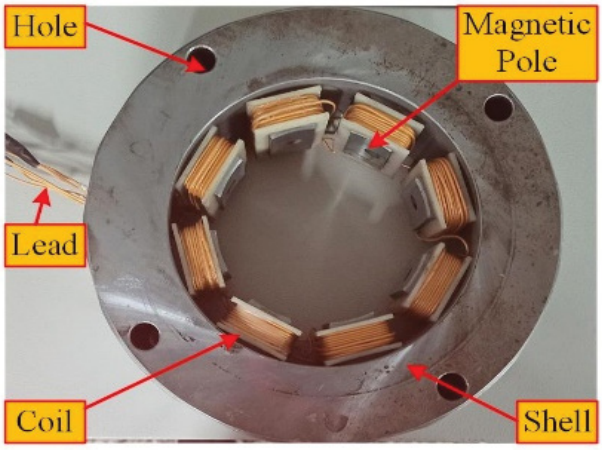

Fig. 4. Radial unit of MLDSB.

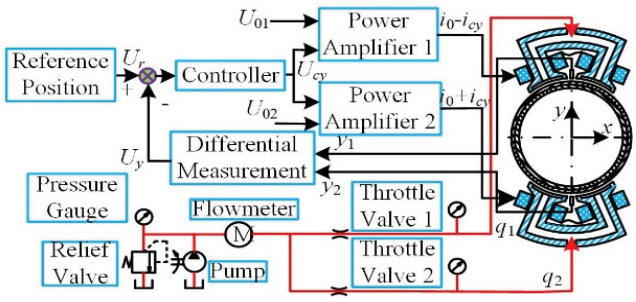

Fig. 5. Single supporting system of MLDSB.

adjusted by the hydrostatic supporting system and electromagnetic system, and then it returns to the equilibrium position gradually.

With the development of bearing-rotor system towards large-scale and high-power, the design gap between the rotor and stator becomes smaller and smaller, which makes the liquid film thickness of MLDSB reduced by 10 times compared with the traditional electromagnetic air gap.

Moreover, the clearance-rubbing fault between magnetic pole and magnetic sleeve can be caused easily by the eccentricity, crack, bending, improper assembly of rotor, the coating cracks and falls off, and then the operation stability and reliability of MLDSB can be reduced significantly [7].

Nikiforov [8] researched transitional processes in the rotor-stator system when the rotor becomes abruptly unbalanced, and the rotor rotates slower or faster than its critical speed while the torque is standard for turbine characteristics. It is shown that rotor in contact can operate relatively safely within a few fractions of a second under immense dynamic load affecting both the rotor and the stator.

Yu et al. [9] established a time-varying wear model based on the L-N model and experimental observations. The effects of both distributed and localized defects are modeled under the excitation from the system itself. The research shows that this model provides a better understanding for the performance evolution of rotor systems during the service period. And this model is also applicable for system fault diagnosis and health monitoring.

Xu et al. [10] established kinetic differential equations of rub-impact under dry rubbing condition by utilizing Hertz contact theory and Coulomb model. Meanwhile, fault dynamic characteristics and impact of rubbing clearance on rotor vibration were analyzed. The results show that, during the process of rub-impact, the spectrums of rotor vibration are complicated and multiple combined frequency components of inner and outer rotor fundamental frequencies are typical characteristic of rub-impact fault for dual-rotor system.

Jin et al. [11] established the calculation model of hybrid lubrication and wear of textured bearing based on statistical model. And the effects of lubrication state transformation and texture on wear process under various working conditions were studied. The results show that, with the increase of eccentricity, the load-carrying capacity and rough peak contact load are increased rapidly, and the inflection point of friction coefficient appears. With the further wear of sliding bearings, the surface texture can play a role in reducing wear.

Zhao et al. [12] established the dynamic model of rubbing fault related to single disk rotor with sliding bearing based on BP neural network and influence function method. The results show that the recognition rate in term of single feature is positively correlated with the value of distinguishing function. The recognition effect of combined features is better than that of single feature, meanwhile the recognition effect of combined features selected in high distinguishing region.

To sum up, due to the coupling and interfere between the electromagnetic system and the hydrostatic system of MLDSB, its supporting mechanism and law are different from the traditional bearing – rotor system [13]. And then the supporting characteristics are the internal foundation and prerequisite for the safe and stable operation. Therefore, a new method for soft-measurement of wear of magnetic pole is presented, and the expressions of bearing stiffness and damping in the magnetic pole coating-wear mode and the dynamic equation of two DOF rubbing system are established. The bearing characteristics and dynamic behavior of bearings under different wear of magnetic poles conditions were studied. Finally, the performance of the system is re-evaluated by means of electromagnetic adjustment.

2. Rubbing dynamic model under wear of magnetic poles

Due to the small clearance-rubbing time, the assumptions can be shown as follows [14].

- There is local elastic collision and Coulomb friction between magnetic pole and magnetic sleeve.
- The small gap between two magnetic poles can be ignored.
- The frictional thermal effect between magnetic pole and magnetic sleeve can be ignored.
- The winding leakage, marginal magnetic flux, vortex loss, magnetic material saturation, coupling effect between magnetic poles can be ignored.
- The inertial force and viscous pressure characteristics of the liquid are ignored.

Clearance-rubbing phenomenon of MLDSB can be shown as Fig. 6 [4] o, o_1, P_T, P_N, α, w_s, e are respectively center of stator, center of rotor, tangential rubbing force, radial rubbing force, angle between rubbing point and x-axis, rotation angle, radial displacement [15].

The mathematical expression of rubbing force P_N and P_T can be shown as follows:

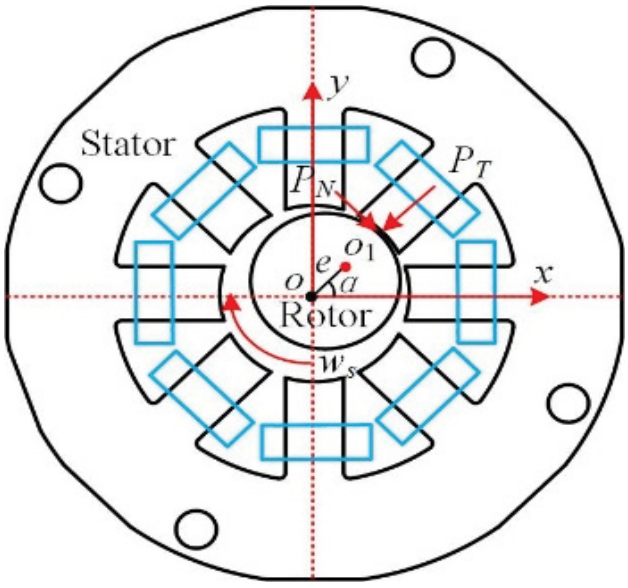

Fig. 6. Clearance-Rubbing Model of MLDSB.

$$\begin{cases} P_N = \left(e - h_0\right)k_c \\ P_T = fP_N \end{cases} \quad e = \sqrt{x^2 + y^2} \geq h_0 \tag{1}$$

where h_0 is liquid film thickness, k_c is radial stiffness of stator, f is friction coefficient.

Decompose Eq. (1) in x-axis and y-axis and transform into dimensionless form as Eq. (2) [16].

$$\begin{Bmatrix} f_X \\ f_Y \end{Bmatrix} = -\left(1 - \frac{h_0}{e}\right)h_0 k_c \begin{bmatrix} 1 & -f \\ f & 1 \end{bmatrix} \begin{Bmatrix} X \\ Y \end{Bmatrix} \tag{2}$$

where f_X is rubbing force of x-axis, f_Y is rubbing force of y-axis.

3. Supporting performance under wear condition

The radial element of MLDSB contains 8 magnetic poles [17]. Two adjacent poles are used in pairs as shown in Fig. 7.

Due to wear of magnetic poles, the thickness of liquid film is increased and the stiffness and damping of the support are reduced, and then the probability and degree of rubbing are aggravated. Therefore, the supporting performance under the wear condition is studied [18].

The initial design parameters of MLDSB are shown in Table 1.

3.1. Supporting stiffness and damping under wear condition

3.1.1. Symmetrical wear in the y-direction (magnetic pole group 3, 4)

Assuming that the wear condition of magnetic pole group 3, 4 are the same and the liquid film thickness increases, the expressions of the bearing stiffness and damping are shown as follows [19].

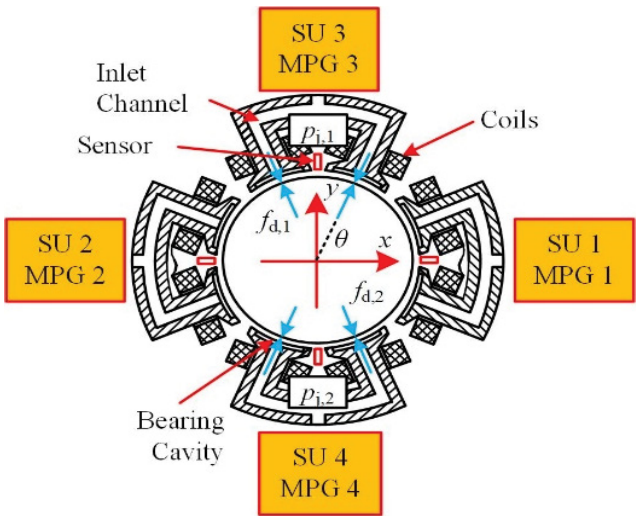

Fig. 7. Force diagram of radial element.

$$\begin{cases} h_3 = h_4 = 1 + \dfrac{s}{h_0} \\ j_y = \dfrac{6A\lambda h^2 \cos\theta}{h_0\left(\lambda h_3^3 + 1\right)^2} \\ c_y = 2\dfrac{B}{h_3^3} \end{cases} \tag{3}$$

According to Table 1, the curve of supporting stiffness and damping with wear amount increasing from 0 to 10 μm can be obtained as shown in Fig. 8.

According to Fig. 8, with the increase of wear amount, the hydrostatic stiffness and damping decrease, while electromagnetic stiffness and damping remain unchanged, so the total stiffness and damping decrease, the supporting performance is degraded.

3.1.2. Unilateral wear in the y-direction (magnetic pole group 3)

Similarly, assuming only magnetic pole group 3 is worn, the stiffness and damping can be expressed as follows [20].

Table 1
Initial parameters of MLDSB

Parameters	Value
Biasing circuit i_0	1 Å
Supply pressure p_s	0.1 MPa
Throttling ratio β	2
Viscosity μ	1.3×10^{-3} Pa·s
Mass of rotor m	4 kg
Air permeability μ_0	$4\pi \times 10^{-7}$ H/m
Supporting cavity area A_e	416 mm²
Extrusion area A_b	56 mm²
Film thickness h_0	50 μm
Angle θ	22.5°
Flow coefficient $\overline{B}$	0.71
Pole area S	1,080 mm²
Turns per coil N	50
Fluidic resistor R_{h0}	1.5×10^{-10} N s/m
Friction coefficient f	0.2
Stator stiffness k_c	6×10^7 N/m
Eccentric mass e	1.3×10^{-5} m
Initial phase angle α	π/4 rad
External load F_{x0}	0
External load F_{y0}	40 N
Proportionality coefficient P_{x0}	12,000
Proportionality coefficient P_{y0}	14,000
Differential coefficient D_{x0}	0.5
Differential coefficient D_{y0}	0.5

$$\begin{cases} h_3 = 1 + \dfrac{s}{h_0} \\ h_4 = 1 \\ j_y = \dfrac{3A\lambda\cos\theta}{h_0}\left[\left(\dfrac{h_3}{\lambda h_3^3 + 1}\right)^2 + \left(\dfrac{h_4}{\lambda h_4^3 + 1}\right)^2\right] \\ c_y = B\left(h_3^{-3} + h_4^{-3}\right) \end{cases} \tag{4}$$

According to Table 1, the curve of supporting stiffness and damping with wear amount increasing from 0 to 10 μm can be obtained as shown in Fig. 9.

According to Fig. 9, the hydrostatic stiffness and damping decrease with the increase of wear, and the degree of wear under symmetrical wear is obviously lower than symmetrical wear. With the increase of wear, the electromagnetic stiffness and damping remain unchanged, while the total stiffness and damping decrease. In addition, the supporting performance decreases.

Meanwhile, unilateral wear of magnetic pole group will also lead to nonlinear terms in the mathematical model and affect its operation stability.

3.2. Rotor displacement under different wear condition

Displacement of the rotor are analyzed under different wear conditions in fourth-order Runge–Kutta method [21].

3.2.1. Displacement response without wear

When wear amount is s = 0, the displacement of rotor with rotation speed is shown as Fig. 10.

According to Fig. 10, as rotate speed increases, the displacement changes from positive to negative. When rotation speed is about 9.2 krpm, the displacement reached a maximum value without rubbing phenomenon. Secondary wear of magnetic pole does not happen.

Table 2
Short names and full names

Short names	Full names
MPG	Magnetic pole group
SU	Supporting unit
HS	Hydrostatic stiffness
ATS	Adjusted total stiffness
AES	Adjusted electromagnetic stiffness
TS	Total stiffness
ES	Electromagnetic stiffness
HD	Hydrostatic damping
ATD	Adjusted total damping
AED	Adjusted electromagnetic damping
TD	Total damping
ED	Electromagnetic damping

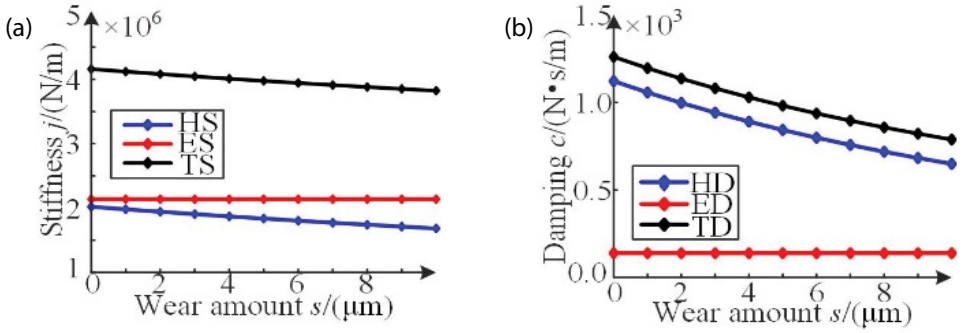

Fig. 8. Supporting performance under symmetrical wear condition: (a) stiffness curve with wear amount and (b) damping curve with wear amount.

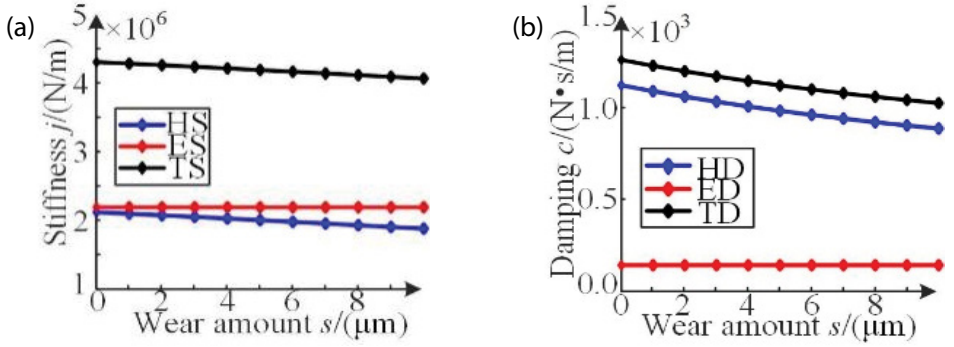

Fig. 9. Supporting performance under unilateral wear condition: (a) curve of stiffness with wear amount and (b) curve of damping with amount of wear.

3.2.2. Symmetrical wear in the y-direction

Similarly, assuming that wear condition of magnetic pole group 3, 4 are the same, the displacement of rotor with rotation speed is shown as Fig. 11.

According to Fig. 11, as rotate speed increases, the displacement changes from positive to negative. When the range of rotation speed is (9, 13) krpm and the range of wear amount is (3, 6) μm, displacement of rotor increases continuously and there is a slight intermittent rubbing phenomenon. As the wear increased to a range of (6, 10) μm, the displacement reached a maximum value with obvious bifurcation and chaos characteristics. The rubbing phenomenon is more serious in this condition, the maximum dimensionless rubbing force reaches 4.3. And it is very likely to cause secondary wear of magnetic pole coating.

3.2.3. Symmetrical wear in x and y-direction

Assuming that wear condition in the *x* and *y*-direction are the same, variation rule of rotor displacement with rotation speed is shown as Fig. 12.

According to Fig. 12, as rotate speed increases, the displacement changes from positive to negative. When the range of rotation speed is (9, 11) krpm and the range of wear amount is (4, 6) μm, displacement of rotor shows slight bifurcation and chaos characteristics and there is no rubbing phenomenon. As the wear increased to a range of

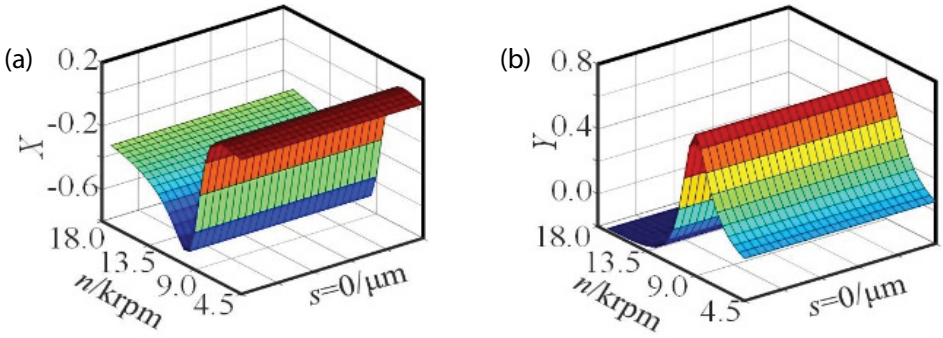

Fig. 10. Displacement of rotor with rotation speed without wear: (a) *s-n-X* diagram and (b) *s-n-Y* diagram.

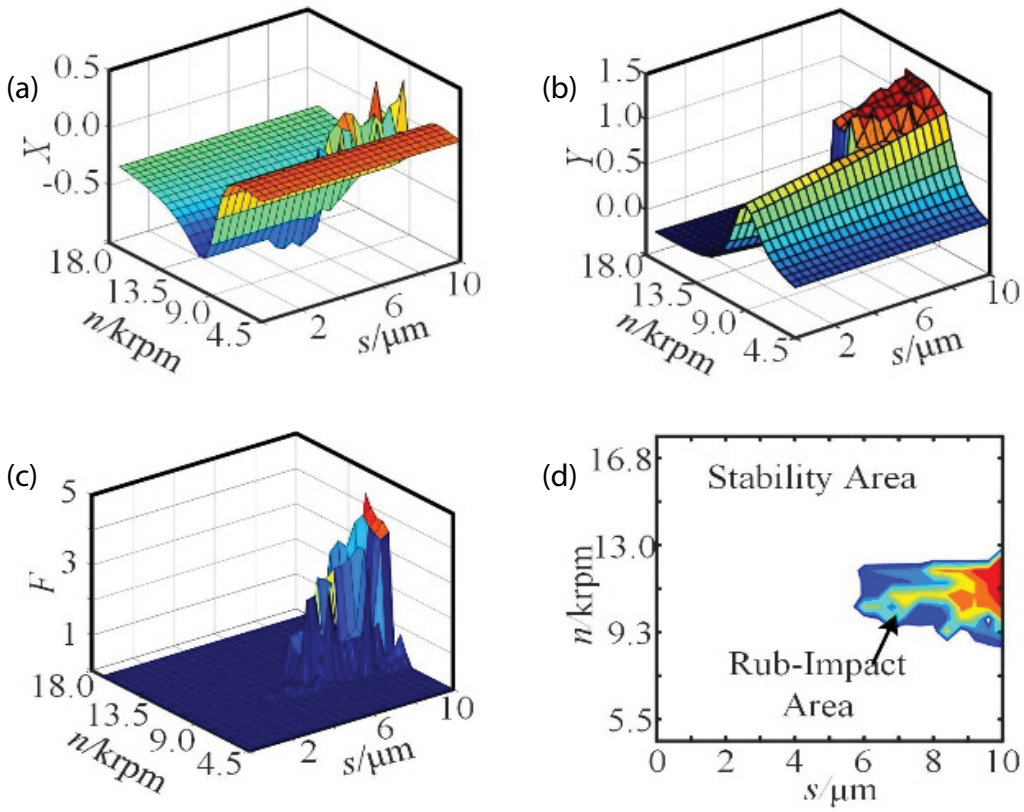

Fig. 11. Response of rotor displacement to symmetrical wear in *y*-direction: (a) *s-n-X* diagram, (b) *s-n-Y* diagram, (c) *s-n-F* diagram, and (d) *s-n* diagram.

(6, 10) μm, the displacement reached a maximum point with obvious bifurcation and chaos characteristics. The rubbing phenomenon is more serious in this condition. And it is very likely to cause secondary wear of magnetic pole coating.

3.2.4. Unilateral wear in the y-direction

Assuming only magnetic pole group 3 is worn, variation rule of rotor displacement with rotation speed is shown as Fig. 13.

According to Fig. 13, the rotor maintains single period of operation throughout operation areas. As rotate speed increases, the displacement changes from positive to negative. When rotation speed around 9.2 krpm, the displacement reached a maximum value with no rubbing phenomenon. Secondary wear of magnetic pole coating does not happen.

3.2.5. Unilateral wear in x and y-direction

Assuming only magnetic pole group 1, 3 are worn, variation rule of rotor displacement with rotation speed is shown as Fig. 14.

According to Fig. 14, as rotate speed increases, the displacement changes from positive to negative. When the range of rotation speed is (9, 11) krpm and the range of wear amount is (3, 5) μm or (6, 9) μm, the displacement reached a maximum value with slight bifurcation and chaos characteristics. The rotor is rubbing in this condition. And it is very likely to cause secondary wear of the magnetic pole.

To sum up, stability comparison of MLDSB under different rubbing conditions are shown as Table 3.

According to Table 3, symmetrical wear is more serious than unilateral wear. In addition, due to the increase of liquid film gap caused by the wear of magnetic poles, the degree of rubbing is the most serious in *y*-direction

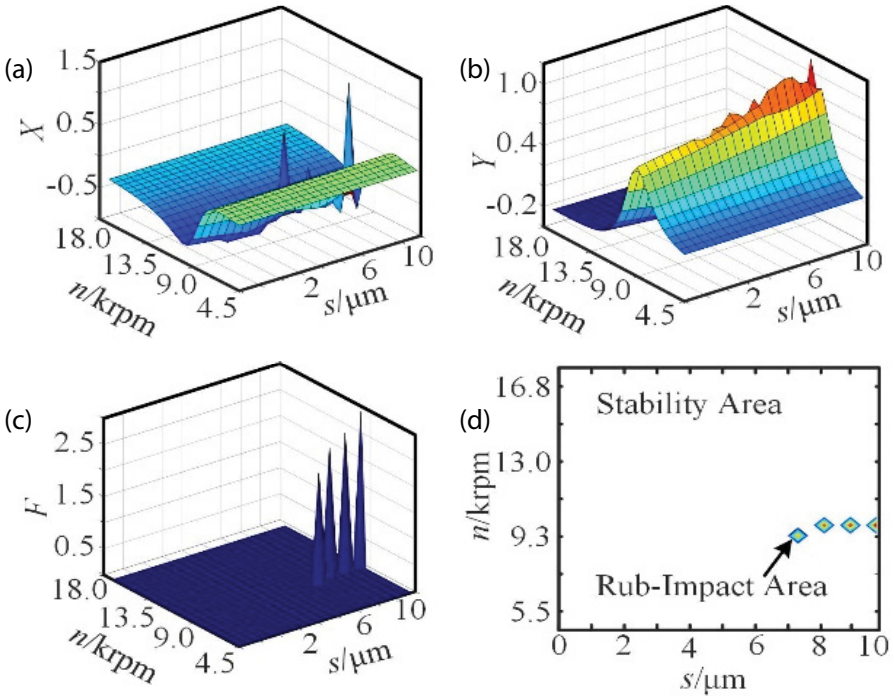

Fig. 12. Response of rotor displacement to symmetrical wear in *x* and *y*-direction: (a) *s*-*n*-*X* diagram, (b) *s*-*n*-*Y* diagram, (c) *s*-*n*-*F* diagram, and (d) *s*-*n* diagram.

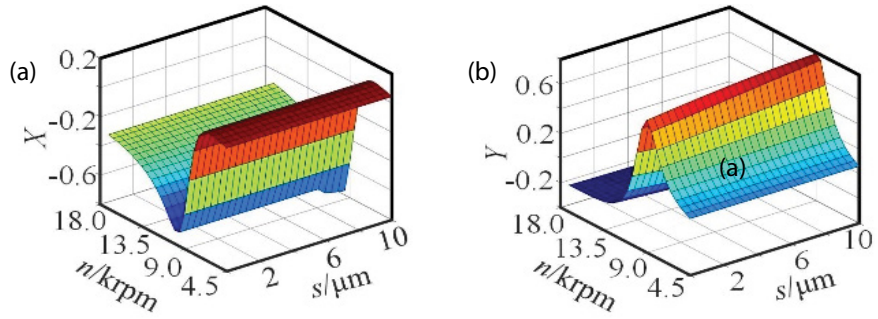

Fig. 13. Response of rotor displacement to unilateral wear in *y*-direction: (a) *s*-*n*-*X* diagram and (b) *s*-*n*-*Y* diagram.

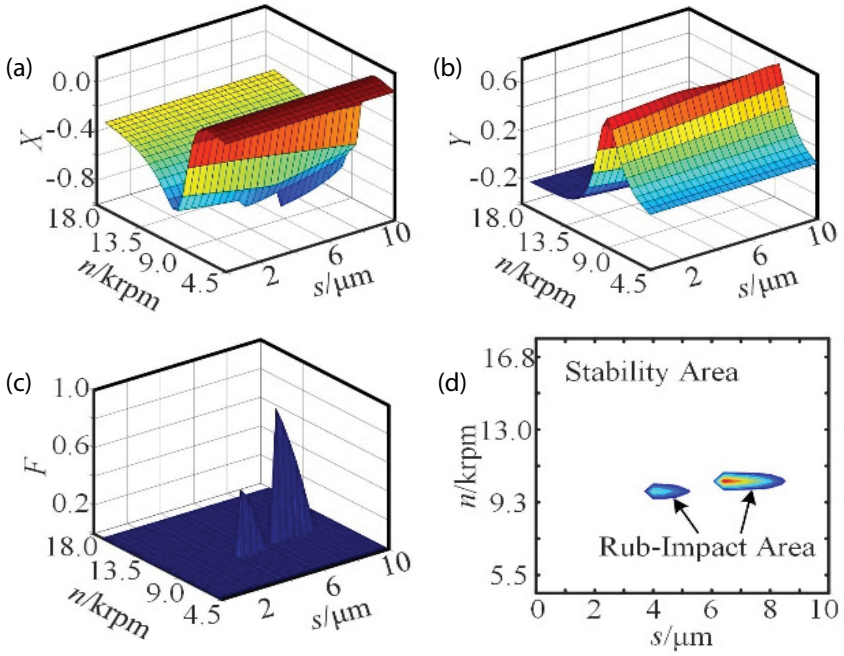

Fig. 14. Response of rotor displacement to unilateral wear in x and y-direction: (a) s-n-X diagram, (b) s-n-Y diagram, (c) s-n-F diagram, and (d) s-n diagram.

Table 3
System stability under different wear conditions

Wear condition	Motion rule	Rubbing conditions
Unworn	Single period	No rubbing
Symmetrical wear in y-direction	Chaos	Serious rubbing
Symmetrical wear in x and y-direction	Multi-period	Slight rubbing
Unilateral wear in y-direction	Single period	No rubbing
Unilateral wear in x and y-direction	Multi-period	Serious rubbing

symmetrical wear. The rubbing and secondary wear of magnetic poles is caused easily by the uneven distribution of the liquid film gap, and then the unstable operation and chaos of the rotor can be aggravated.

To sum up, MLDSB in the start-stop stage is easy to cause wear of magnetic pole group, seriously affecting the safe and stable operation of the system, and the phenomenon of clearance rubbing occurs, which should be adjusted and controlled to avoid rub behavior.

4. Soft measurement of magnetic pole group wear

4.1. Idea of soft measurement

Due to the complex structure, inconvenience of disassembly and installation of MLDSB, it is difficult to monitor and measure the wear state of magnetic poles in real time. Therefore, a soft measurement method by detecting the flow and pressure of hydrostatic system is proposed as follows.

- The flow Q_0 and pressure p_{r0} of the supporting unit under unworn condition are measured.
- The flow Q and pressure p_r of the supporting unit under wear condition are measured.
- According to the flow and pressure of the supporting unit under unworn and wear conditions, the wear amount s of magnetic pole is solved inversely.

4.2. Calculation procedure of soft measurement

- Assuming that constant-pressure supplying model is adopted by hydrostatic system, each supporting unit under unworn condition can be expressed as follows [22].

$$\begin{cases} R_{h0} = \dfrac{\mu}{\bar{B}h_0^3} \\ Q_0 = \dfrac{p_s}{R_g + R_{h0}} \\ p_{r0} = \dfrac{p_s R_{h0}}{R_g + R_{h0}} \end{cases} \tag{5}$$

where p_s is system pressure, R_g is fluidic resistor of throttle valve, R_{h0} is initial fluidic resistor of bearing cavity, μ is lubricating fluid viscosity, h_0 is initial thickness of liquid film, Q_0 is Initial supply flow, $\bar{B}$ is flow coefficient, p_{r0} is Initial pressure of supporting cavity.

- Assuming wear amount of magnetic pole is s, the supporting unit can be expressed as follows [23].

$$\begin{cases} R_h = \dfrac{\mu}{\bar{B}\left(h_0 + s\right)^3} \\ Q = \dfrac{p_s}{R_g + R_h} \\ p_r = \dfrac{p_s R_h}{R_g + R_h} \end{cases} \tag{6}$$

where R_h is fluidic resistor of supporting cavity, Q is supply flow, p_r is pressure of supporting cavity.

- According to Eqs. (6) and (7), the resistance R_h, flow Q and pressure p_r change with wear degrees of coating. Therefore, the expressions of wear amount, flow and pressure can be solved reversely as follows [24].

$$R = \sqrt{\frac{\mu^2}{4\bar{B}^2 R_g^2} - \frac{p_s^3}{27Q^3 R_g^3}} - \frac{\mu}{2\bar{B}R_g} \tag{7}$$

$$\begin{cases} s_Q = R^{\frac{1}{3}} + \dfrac{p_s}{3QR_g R^{\frac{1}{3}}} - h_0 \\ s_p = \left(\dfrac{\mu\left(p_s - p_r\right)}{p_r \bar{B} R_g}\right)^{\frac{1}{3}} - h_0 \end{cases} \tag{8}$$

where s_Q and s_p are derived from flow and pressure respectively.

- The average of wear amount of magnetic poles is obtained as follows [25].

$$s = \frac{s_Q + s_p}{2} \tag{9}$$

According to Table 1, the curve of flow and pressure of supporting unit with wear amount increasing from 0 to 10 μm can be obtained as shown in Fig. 15.

According to Fig. 15, flow increases and the pressure decreases with wear amount increasing. Therefore, wear amount can be obtained by real-time measurement of flow and pressure. The method can provide a theoretical basis for the safe and stable operation.

5. Adjustment of supporting performance under wear condition

5.1. Adjustment strategy under wear condition

Supporting stiffness and damping can be reduced due to wear of magnetic poles [26]. The change of stiffness and damping can be compensated by adjusting PD control parameters, and performance of MLDSB can be restored as before. The regulation strategy is as follows [27].

- According to Table 1, the numerical solutions of stiffness j_0 and damping c_0 of the hydrostatic supporting system are obtained.
- According to the above soft-measurement method, the specific value of wear amount is obtained and substituted into Eq. (4), the numerical solutions of real-time stiffness j_y and damping c_y of the hydrostatic supporting system are obtained.
- According to the difference value of numerical solution of the above two wear conditions, the numerical solutions of electromagnetic $P_{tx,ty}$ and $D_{tx,ty}$ that need to be adjusted are solved inversely.

5.2. Determination of electromagnetic control parameters

- Under unworn condition, the hydrostatic stiffness j_0 and damping c_0 are shown respectively in Eq. (10) [28].

$$\begin{cases} j_0 = 12A_e p_s \lambda \cos^2\theta / B^2 h_0 \\ c_0 = 4A_b A_e R_{h_0} \cos^2\theta \end{cases} \tag{10}$$

- According to the wear amount, the real-time hydrostatic stiffness and damping are shown in Eq. (11).

$$\begin{cases} h_i = 1 + \dfrac{\varepsilon_i}{h_0}, h_j = 1 + \dfrac{\varepsilon_j}{h_0} \\ j_{x,y} = \dfrac{3A\lambda\cos\theta}{h_0}\left[\left(\dfrac{h_i}{\lambda h_i^3 + 1}\right)^3 + \left(\dfrac{h_j}{\lambda h_j^3 + 1}\right)^3\right], c_{x,y} = B\left(h_i^{-3} + h_j^{-3}\right) \end{cases} \tag{11}$$

where $i = 1$, $j = 2$ in x-direction; $i = 3$, $j = 4$ in y-direction.

- According to the above expressions under wear condition, the expressions of electromagnetic control parameters ($P_{tx,ty}$, $D_{tx,ty}$) that need to be set are solved inversely as follows in Eq. (12).

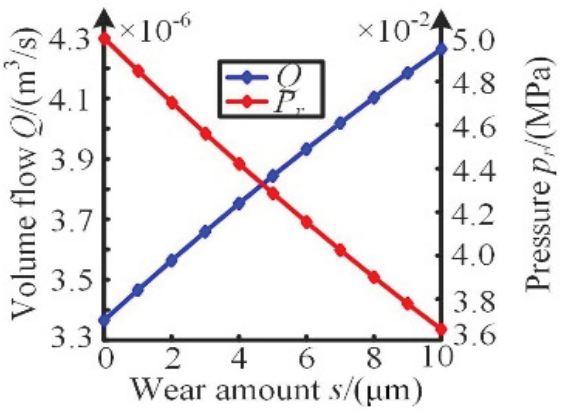

Fig. 15. Flow and pressure of supporting unit with wear amount.

$$\begin{cases} P_{tx,ty} = k_t\left(j_0 - j_{x,y}\right) + P_{x0,y0} \\ D_{tx,ty} = k_t\left(c_0 - c_{x,y}\right) + D_{x0,y0} \end{cases} \tag{12}$$

where k_t is slope of the electromagnetic control, $k_t = \delta_0^2 / \left(8 i_0 k \cos\theta\right)$; P_{x0}, P_{y0}, D_{x0}, D_{y0} are electromagnetic control parameters under unworn condition in x and y-direction.

5.3. Comparison before and after adjustment

The real-time stiffness and damping obtained by calculating the wear amount are substituted into Eq. (11) to calculate the numerical solution of electromagnetic control parameters [29]. The stiffness, damping and rotor displacement response rules after adjustment are presented with Software MATLAB [30], as shown in Fig. 16.

Compare with Figs. 8 and 16a & b, as wear amount increases, the electromagnetic stiffness and damping increase in order to compensate the loss of the supporting stiffness and damping of hydrostatic supporting system, and then the total stiffness and damping of MLDSB remain stable.

Compare with Figs. 11 and 16c & d, the bifurcation and chaos of rotor's displacement do not occur, the response of the rotor is periodical motion the rotor throughout the whole rotation scope without rubbing phenomenon and secondary wear.

According to the different wear amount in Eq. (11), the parameters of the electromagnetic system can be preset in order to improve supporting stiffness and damping as Fig. 17 and then the secondary wear are prevented [31].

The dynamic regulation process can be intuitively analyzed by detecting the change of controlling current [32]. Wear amount and rotor displacement of symmetrical wear in y-direction are taken as the study plane [33], and three-dimensional model of bias current is established as shown in Figs. 18 and 19.

According to Figs. 18 and 19, the current changes complexly with the irregular peaks and troughs before adjustment, while the current is simple and rotor can keep stable after adjustment.

6. Experimental research

6.1. Introduction of MLDSB testing table

MLDSB Testing System is composed of electronic control system, hydrostatic system and bearing body as shown in Fig. 20, and its principle is shown in Fig. 21.

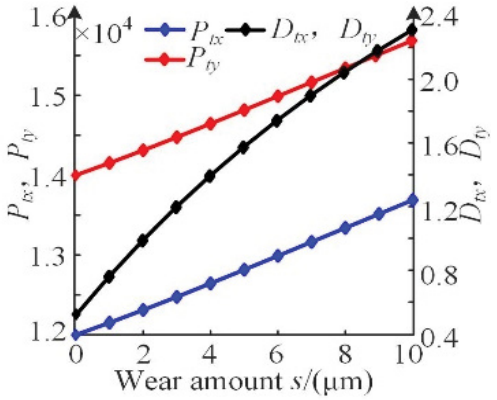

Fig. 17. Control parameters under wear condition.

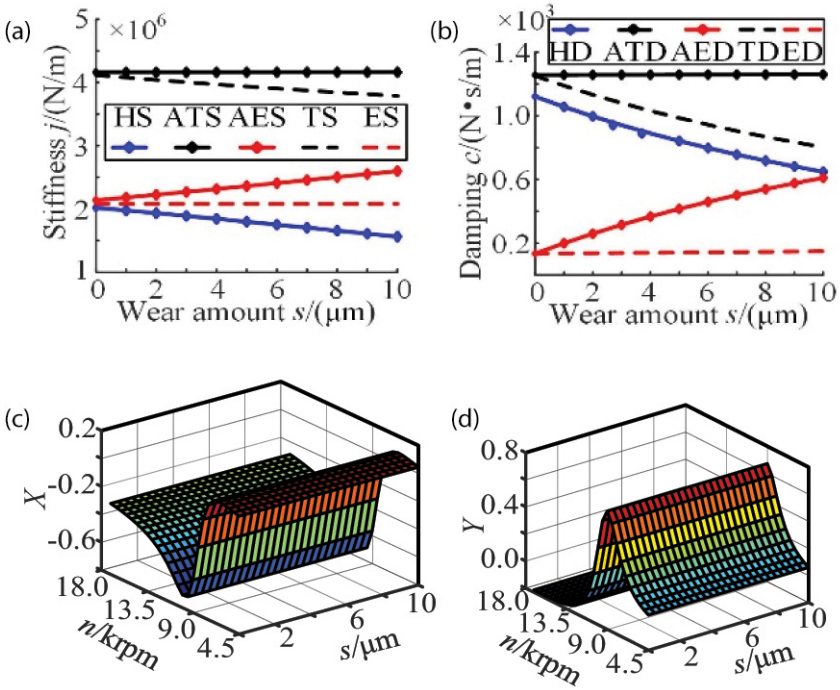

Fig. 16. System response after adjustment: (a) supporting stiffness, (b) supporting damping, (c) s-n-X diagram, and (d) s-n-Y diagram.

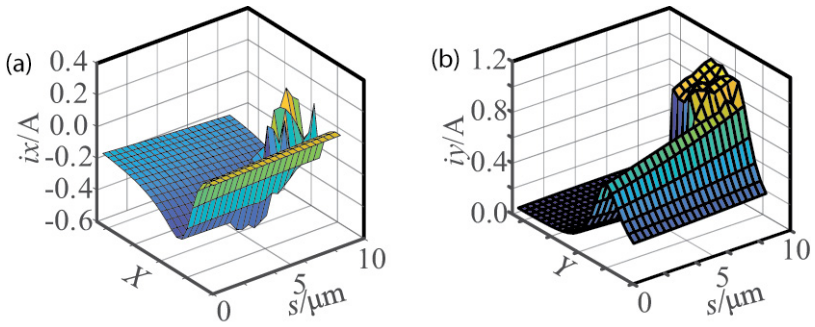

Fig. 18. Bias current before adjustment: (a) s-X-i_x diagram and (b) s-Y-i_y diagram.

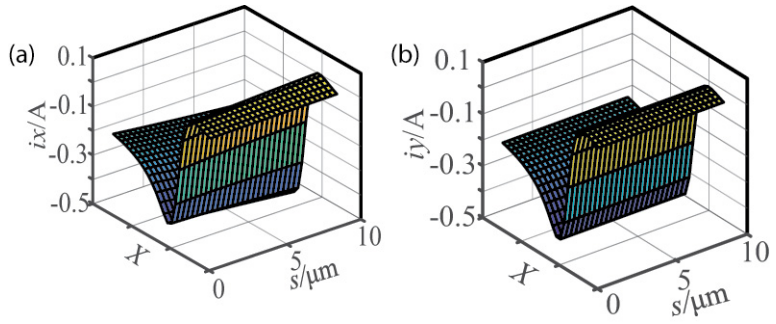

Fig. 19. Bias current after adjustment: (a) s-X-i_x diagram and (b) s-Y-i_y diagram.

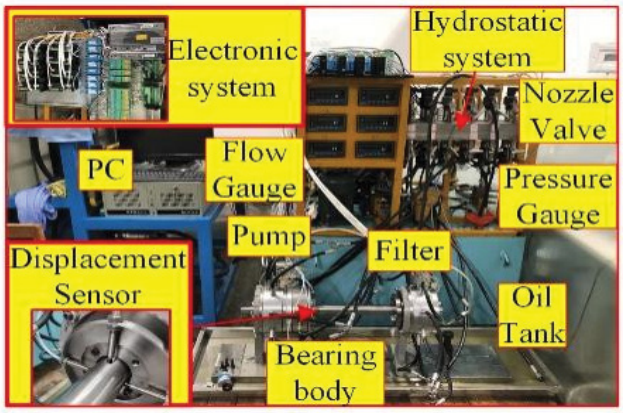

Fig. 20. Photo of MLDSB testing system.

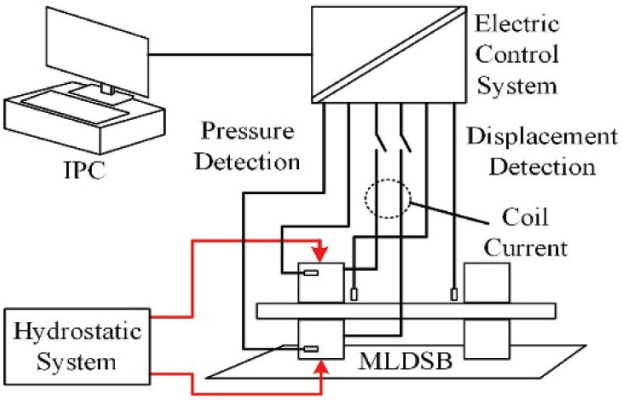

Fig. 21. Principle of MLDSB testing table.

Constant pressure supporting model is adopted in hydrostatic system, and its flow is adjusted by needle valve. The closed-loop position control system is adopted in electronic control system, and its current is adjusted by PD controller. The principle of hydrostatic system and electronic control system are shown in Fig. 5, and bearing body is shown in Fig. 2.

The component's parameters of MLDSB Testing System is shown as follows.

- Hydraulic pump, model TGPVL4-200SH, manufacturers for Taixing Hongsheng Hydraulic Co., Ltd., China, pressure 14 MPa, flow 16 L/min, rotate speed 1,450 r/min.
- Relief valve, model DBD-H-6-P-10-B-NG10, manufacturers for Beijing Huade Hydraulic Industrial Group Co., Ltd., China, pressure 10 MPa, size 6 mm.
- Nozzle valve, model A7-2-KL2-0KL20-PTFE, manufacturers for Shanghai Hawk Fluid Control Co., Ltd., China, size 6 mm.
- Flow gauge, model LWGY-S, manufacturers for Nanjing Detair Instrument & Electromechanical Equipment Co., Ltd., China, pressure 2 MPa, flow 120–2,400 mL/min, and accuracy 2%.
- Pressure gauge, model HSTL-802, manufacturers for Beijing Huakong Xingye Technology Development Co., Ltd., China, pressure 10 MPa, accuracy 0.25%.
- Displacement gauge, model VB-Z9900, manufacturers for Shanghai Ann Electronic Technology Co., Ltd., China, range for 4 mm, accuracy 1.5%.
- Coil, materials for Cu, diameter 1.0 mm, electrical resistivity 0.02240 Ω/m, length 25 m.
- PC, model IPC-610L, manufacturers for Taiwan Advantech Co., Ltd., mainboard AIMB-705BG, CPU I5-6500.

- Output card, model NI6723, manufacturers for America NI instruments Co., Ltd., eight channels output.
- Input card, model PCI1716, manufacturers for Taiwan Advantech Co., Ltd., 16 channels input.
- 12 V Power, model S1500-12, manufacturers for China Meanwell Group Co., Ltd., voltage 12 V, current 125 A, power 1,500 W.
- Power amplifier, model AQMD3620NS-A2, manufacturers for Chengdu Aikong Electric Technology Co., Ltd., power 400 W, input voltage 36 V, current 16 A.

6.2. Testing procedure

Assume that magnetic pole coating does not wear, the thickness of liquid film can be adjusted by changing the different magnetic sleeves. In the experiment, the rotor is suspended to the center of the bearing, and the wear amount of magnetic pole can be determined by the difference between the liquid film thickness and the reference magnetic sleeves. In addition, y-direction is selected as the research subject. The specific experimental steps are shown as follows:

- The inner diameter of the stator and the outer diameter of three magnetic sleeves are measured. The first magnetic sleeve is selected as the standard to determine the reference liquid film thickness h_0.
- Start hydrostatic system and the electromagnetic system and suspend the rotor to the balance position (bearing center).
- Record the pressure of upper and lower supporting cavity. Replace three magnetic sleeves, record the data separately.
- The pressure of upper and lower supporting cavity is put into follow equation, and the wear of magnetic poles is solved as follows.

$$s_p = \left(\frac{\mu\left(p_s - p_r\right)}{p_r \bar{B} R_g} \right)^{1/3} - h_0 \tag{13}$$

6.3. Experimental results of soft-measurement wear amount of magnetic poles

In the experiment, three groups of magnetic conductors with different clearances were selected for the experiment. The inner diameter of the stator and the outer diameter of three magnetic sleeves are measured. The first magnetic sleeve is selected as the standard to determine the reference liquid film thickness h_0. The equivalence of different size of magnetic guide sleeve is regarded as different wear amount of the same magnetic guide sleeve. Pictures of three groups of magnetic conductors with different clearances are shown in Fig. 22.

During the experiment, the first magnetic sleeve is selected as the reference, and experimental data are shown in Table 4.

6.3.1. Manual measurement of wear of magnetic sleeve

The inner diameter of stator and the outer diameter of magnetic sleeve are measured manually as shown in Tab.5.

According to Table 5, there are different wear amount in three magnetic sleeves, and the deviation between real thickness and standard thickness of liquid film can be resulted.

6.3.2. Soft measurement of wear amount of magnetic sleeve

The rotor is adjusted to the center of the bearing through the electronic control system, and the rotor displacement, pressure of oil cavity after stabilization can be shown in Figs. 23–26.

According to Figs. 23–26, when first magnetic sleeve is installed, the pressure of upper and lower supporting

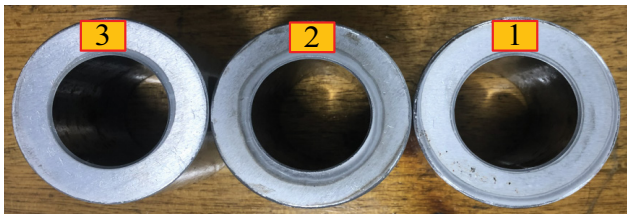

Fig. 22. Different magnetic sleeve.

Table 4
Experimental data

Oil pressure p_s (MPa)	0.6
Diameter of stator R_0 (mm)	60.440
Diameter magnetic sleeve R_3 (mm)	60.350
Thickness of liquid film h_0 (μm)	45
Throttle fluid resistance R_{g0} (N s/m)	1.722×10^{12}

Table 5
Liquid film thickness and wear of magnetic pole

Number	Inner diameter of stator (mm)	Outer diameter of magnetic sleeve (mm)	Thickness of liquid film (μm)		Magnetic sleeve wear amount (μm)	Magnetic sleeve wear rate
			Standard	Real		
1	60.440	60.350	45	45	0	0%
2	60.440	60.342	45	49	4	8.2%
3	60.440	60.344	45	48	3	6.3%

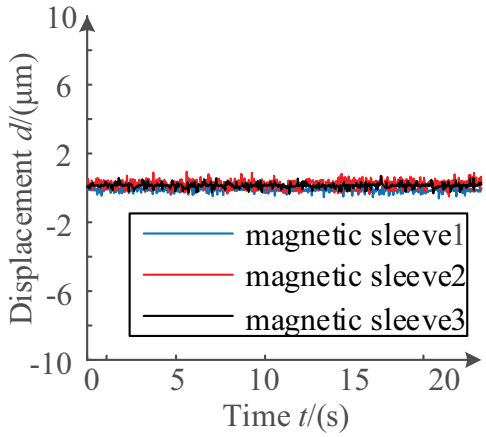

Fig. 23. Rotor displacement with different magnetic sleeve.

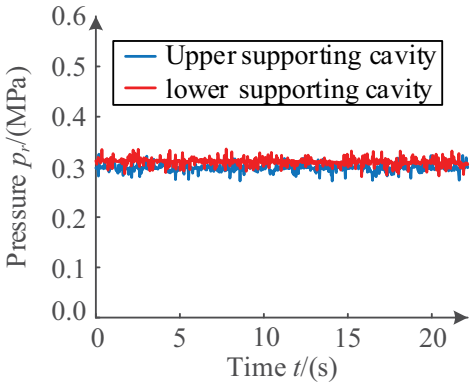

Fig. 24. Supporting cavity pressure with first magnetic sleeve.

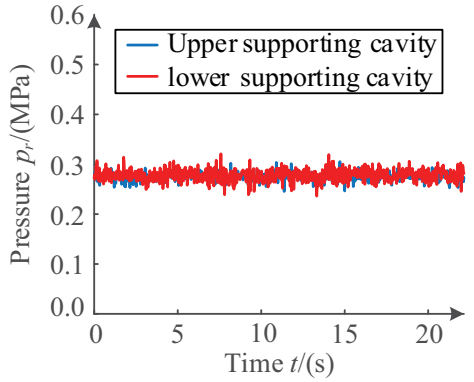

Fig. 25. Oil cavity pressure with second magnetic sleeve.

cavity are respectively 0.30 and 0.31 MPa. When second one is installed, the pressure of upper/lower supporting cavity are stable at 0.27 MPa. When third one is installed, the pressure of upper/lower supporting chamber are stable at 0.28 MPa.

The pressure in Figs. 23–26 are imported into Eq.12 to obtain liquid film thickness of upper and lower supporting cavity and the wear amount of magnetic pole as shown in Table 6.

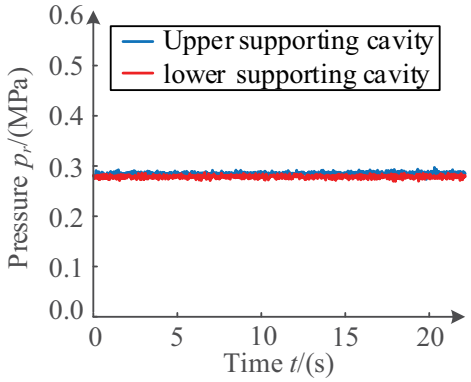

Fig. 26. Oil cavity pressure with third magnetic sleeve.

Table 6
Soft measurement of magnetic sleeve wear

		Liquid film thickness		Wear amount of magnetic pole (μm)	
		Soft measurement			
Number	Standard	Upper	Lower	Upper	Lower
1		45.000	44.011	0	–0.989
2	45	48.113	48.113	3.113	3.113
3		47.048	47.048	2.048	2.048

According to Tables 5 and 6, the error of liquid film thickness obtained by manual measurement and soft measurement are shown in Table 7, and the wear error of magnetic pole are shown in Table 8.

According to Table 7, the liquid film thickness by manual measurement is basically consistent with that obtained by soft measurement, and the error is in the scope of 1 μm. The need of engineering practice can be met.

According to Table 8, the wear amount by manual measurement is basically consistent with that obtained by soft measurement, and the error is in the scope of 1 μm. The need of engineering practice can be met.

7. Conclusion

- Supporting performance and operation stability of MLDSB are reduced by the wear of magnetic poles. Unilateral wear makes the least impact, and secondary wear does not occur. Symmetrical wear makes the most serious impact, and the obvious bifurcation, chaos and secondary wear of magnetic poles can be triggered. The rotor displacement will show bifurcation behavior in advance as the wear amount increases.
- A new soft-measurement method is proposed to predict the wear amount of magnetic poles by measuring the pressure and flow of the supporting cavity in real time. It can monitor the wear state of magnetic pole without disassembling and installing MLDSB.
- A control strategy by adjusting the electromagnetic control parameters in real time is proposed to improve the bearing stiffness and damping and to prevent the

Table 7
Soft measurement of magnetic sleeve wear

No.	Film thickness (μm)						
	Manual measurement	Soft measurement		Error (μm)			
		Upper	Lower	Upper	Lower	Average	Percentage
1	45	45.000	44.011	0	–0.989	0.495	1.1%
2	49	48.113	48.113	0.887	0.887	0.887	1.8%
3	48	47.048	47.048	0.952	0.952	0.952	2.0%

Table 8
Soft measurement of magnetic sleeve wear

No.	Pole wear amount (μm)							
	Manual measurement		Soft measurement		Error (μm)			
	Upper	Lower	Upper	Lower	Upper	Lower	average	Percentage
1	0	0	0	–0.989	0	0.989	0.495	/
2	4	4	3.113	3.113	0.887	0.887	0.887	22.1%
3	3	3	2.048	2.048	0.952	0.952	0.952	31.7%

secondary wear of magnetic pole. The control strategy effectively compensates the stiffness and damping loss caused by the wear of magnetic pole group, and improve the supporting performance of MLDSB.

Data availability

No data were used to support this study. We only used computer for simulation. Therefore, we can only provide simulation programming, which can be obtained from the corresponding author upon request.

Conflicts of interest

The author declares that there are no conflicts of interest regarding the publication of this paper.

Acknowledgments

This work was supported by the National Nature Science Foundation of China (No. 52075468); General project of Natural Science Foundation of Hebei Province (No. E2020203052); Youth Fund project of Scientific Research Project of Higher Education in Hebei Province (No. QN2020130); Open Fund of Key Laboratory of Hydraulic Technology in Shaanxi Province (No. YYJS2022KF14) and Basic Innovation Research Cultivation Project of Yanshan University (No. 2021LGZD003).

References

[1] A. Belila, J. El-Chakhtoura, N. Otaibi, G. Muyzer, G. Gonzalez-Gil, P.E. Saikaly, M.C.M. van Loosdrecht, J.S. Vrouwenvelder, Bacterial community structure and variation in a full-scale seawater desalination plant for drinking water production, Water Res., 94 (2016) 62–72.
[2] G.X. Dong, J.F. Kim, J. Kim, E. Drioli, Y.M. Lee, Open-source predictive simulators for scale-up of direct contact membrane distillation modules for seawater desalination, Desalination, 402 (2017) 72–87.
[3] L.S. Andrés, S. Phillips, D. Childs, A water-lubricated hybrid thrust bearing: measurements and predictions of static load performance, J. Eng. Gas Turbines Power, 139 (2017) 72–87.
[4] J. Zhao, W. Yan, Z. Wang, D. Gao, G. Du, Study on clearance-rubbing dynamic behavior of 2-DOF supporting system of magnetic-liquid double suspension bearing, Processes, 8 (2020) 973–988.
[5] T.W. Wu, Influence of bearing friction and wear on dynamic response characteristics of flexibly supported rotor, Atomic Energy Sci. Technol., 54 (2020) 715–724.
[6] J. Zhao, L. Xing, S. Li, W. Yan, D. Gao, G. Du, Impact-rubbing dynamic behavior of magnetic-liquid double suspension bearing under different protective bearing forms, Processes, 9 (2021) 1105, doi: 10.3390/pr9071105.
[7] M. Torkhani, L. May, P. Voinis, Light, medium and heavy partial rubs during speed transients of rotating machines: numerical simulation and experimental observation, Mech. Syst. Sig. Process., 29 (2012) 45–66.
[8] A.N. Nikiforov, Vibroimpact motion, slippage and return of the rotor on the stator, J. Mach. Manuf. Reliability, 41 (2012) 11–19.
[9] H. Yu, Y. Ran, G. Zhang, X. Li, B. Li, A time-varying comprehensive dynamic model for the rotor system with multiple bearing faults, J. Sound Vib., 488 (2020) 115650, doi: 10.1016/j.jsv.2020.115650.
[10] H. Xu, N. Wang, D. Jiang, T. Han, D. Li, Dynamic characteristics and experimental research of dual-rotor system with rub-impact fault, Shock Vib., 6 (2016) 1–11.
[11] L.J. Jin, J.X. Yang, C.G. Li, Numerical coupled model of mixed lubrication wear for textured journal bearing, Lubr. Eng., 45 (2019) 64–74.
[12] B.X. Zhao, D.W. Ja, Q. Yuan, P. Li, Q. Ge, Rubbing fault diagnosis of rotor system based on combined feature space in time and time-frequency domains, J. Xi'an Jiaotong Univ., 54 (2019) 1–11.
[13] W.L. Xiong, C. Hu, L. Lv, L.G. Zheng, Research on the influence of controllable restrictor parameters on the characteristics of hydrostatic journal bearings, Chin. J. Mech. Eng., 54 (2018) 63–71.
[14] H. Yu, Y.S. Chen, Q.J. Cao, Nonlinear dynamic behavior analysis for a cracked multi-DOF rotor system, Shock Vib., 33 (2014) 92–98.
[15] S.B. Bulgarevic, M.V. Boiko, K.S. Lebedinskii, Adsorption separation of components of liquid lubricant on rubbing

surfaces under sliding friction, J. Friction Wear, 36 (2015) 534–541.
[16] G.A. Kostyuk, F.V. Shatokhin, A.O. Volokhovskaya, Specific features relating to the motion of a rotor with rubbing against the stator, Therm. Eng., 60 (2013) 628–634.
[17] G. Zhang, Q.Z. Ying, S.P. Liang, Research on nonlinear dynamics of five-DOF active magnetic bearings-rotor system, Chin. J. Mech. Eng., 46 (2020) 15–21.
[18] L. Cheng, G.S. Cheng, J. Yang, Research on the method of automatic repair of bearing wear at high speed, Ship Sci. Technol., 41 (2019) 203–205.
[19] G.Y. Zhang, H.Z. Huang, M. Zhou, K. Chen, J.A. Wei, Nonlinear dynamic model and its stability for the generator rotor with coupling the unbalanced electromagnetic force and the oil film force, Proc. CSEE, 34 (2014) 2406–2413.
[20] B.Y. Sun, R.S. Liang, W. Chen, Control of nonlinear behaviors of an active magnetic Bearing-Rotor system, Noise Vibr. Control, 31 (2011) 11–14.
[21] Z.W. Xie, W.X. Mou, H. Zhou, X. Wang, Variable parameter control of active magnetic bearing rotor system based on rotation speed, J. Vibr. Eng., 25 (2012) 739–744.
[22] Y. Shang, J. Ling, X. Liu, X. Xin, Impact of hydrostatic bearings on the dynamic performance of electric spindle rotor device, Mech. Sci. Technol., 34 (2015) 588–693.
[23] G. Peng, C. Li, C. Cao, J. Hong, Dynamic response and safety design of rotor system with impact excitation, Propul. Technol., 39 (2018) 1111–1121.
[24] P. Kankar, S. Sharma, S. Harsha, Fault diagnosis of ball bearings using machine learning methods, Expert Syst. Appl., 38 (2010) 1876–1886.
[25] J.J. Sinou, A.W. Lees, The influence of cracks in rotating shafts, J. Sound Vib., 285 (2004) 1015–1037.
[26] L. Hou, Y.S. Chen, Z.Y. Lu, Z.G. Li, Bifurcation analysis for 2:1 and 3:1 super-harmonic resonances of an aircraft cracked rotor system due to maneuver load, Springer Netherlands, 81 (2015) 531–547.
[27] G. Jacquet-Richardet, M. Torkhani, P. Cartraud, F. Thouverez, T.N. Baranger, M. Herran, C. Gibert, S. Baguet, P. Almeida, L. Peletan, Rotor to stator contacts in turbomachines. Review and application, Mech. Syst. Sig. Process., 40 (2013) 401–420.
[28] L. Hou, Y.S. Chen, Q.J. Cao, Nonlinear vibration phenomenon of an aircraft rub-impact rotor system due to hovering flight, Commun. Nonlinear Sci. Numer. Simul., 19 (2014) 286–297.
[29] H. Ma, X.Y. Zhao, Y.N. Teng, B.C. Wen, Analysis of dynamic characteristics for a rotor system with pedestal looseness, Shock Vibr., 18 (2011) 13–27.
[30] A.S. Sekhar, Crack detection and monitoring in a rotor supported on fluid film bearings: start-up vs run-down, Mech. Syst. Sig. Process., 17 (2001) 897–901.
[31] K. Lu, Y.L. Jin, P.F. Huang, F. Zhang, H.P. Zhang, C. Fu, Y.S. Chen, The applications of POD method in dual rotor-bearing systems with coupling misalignment, Mech. Syst. Sig. Process., 150 (2020) 1–17.
[32] Y. Ma, H. Liu, Y. Zhu, F. Wang, Z. Luo, The NARX model-based system identification on nonlinear, rotor-bearing systems, Appl. Sci., 7 (2017) 1–15.
[33] A. Alho, C. Uggla, Global dynamics and inflationary center manifold and slow-roll approximants, J. Math. Phys., 56 (2014) 241101–360.